

The Kondo effect in C_{60} single-molecule transistors

Lam H. Yu and Douglas Natelson

Department of Physics and Astronomy, Rice University, 6100 Main St., Houston, TX 77005

(Dated: November 20, 2018)

We have used an electromigration technique to fabricate C_{60} -based single-molecule transistors. We detail the process statistics and the protocols used to infer the successful formation of a single-molecule transistor. At low temperatures each transistor acts as a single-electron device in the Coulomb blockade regime. Resonances in the differential conductance indicate vibrational excitations consistent with a known mode of C_{60} . In several devices we observe conductance features characteristic of the Kondo effect, a coherent many-body state comprising an unpaired spin on the molecule coupled by exchange to the conduction electrons of the leads. The inferred Kondo temperature typically exceeds 50 K, and signatures of the vibrational modes persist into the Kondo regime.

PACS numbers: 73.63.-b,73.23.Hk,72.80.Rj

A transistor with an active region consisting of a single small molecule is the ultimate limit of the miniaturization of three-terminal electronic devices. Such single-molecule transistors (SMTs) have been demonstrated using molecules of C_{60} [1], C_{140} [2], cobalt coordination complexes[3], and divanadium complexes[4]. These SMTs function as single-electron transistors[5, 6], with conduction dominated by Coulomb blockade effects. Because of the small size of the molecules, charging energies and single-particle level spacings in these devices are of the same order (~ 1 eV), and are much larger than those in semiconductor or metal single-electron devices.

Devices incorporating the latter two molecules[3, 4] exhibit signatures of the Kondo effect[7] in their conduction properties. In a single-electron device with a localized unpaired spin, it is possible to observe Kondo physics, the growth of a correlated many-body state comprising the localized spin interacting by antiferromagnetic exchange with the spins of the conduction electrons of the leads. This results in a Kondo resonance, an enhanced density of states of the leads. For dilute magnetic impurities in bulk metals the result is enhanced scattering and therefore a low temperature rise in the resistivity as the Kondo state develops. Conversely in single-electron devices[8, 9, 10, 11] the result is enhanced transmission, manifested as a zero bias peak in the conductance present when $T < T_K$, the Kondo temperature. The Kondo energy scale T_K depends exponentially on the spin-lead coupling, and on the energy of the localized level relative to the Fermi level of the lead conduction electrons. In single-electron devices, Kondo physics has been observed in semiconductor quantum dots[12, 13], carbon nanotubes[14, 15], and the single-molecule transistors incorporating metal ions mentioned above. Kondo temperatures in these latter experiments range from 10 K to 25 K.

In this letter, we report measurements on SMTs incorporating individual C_{60} molecules coupled to gold source and drain electrodes. We describe the fabrication procedure in detail, including the statistics of the conduction properties of the resulting devices and the protocols used

to infer the successful formation of a SMT. We confirm the presence of C_{60} vibrational resonances in devices in the Coulomb blockade regime. In several devices we report observations consistent with Kondo physics. The Kondo temperatures inferred from the transport data typically exceed 50 K, significantly higher than previously reported values in single-electron devices. The data also suggest that signatures of inelastic vibrational processes can persist well into the Kondo regime, evidence of coupling between a vibrational excitation and the coherent many-body state.

The fabrication process is based on the electromigration technique[16] employed in previous SMT investigations[1, 2, 3, 4]. E-beam lithography (EBL) and lift-off processing are used to define 15-60 metal constrictions connected to contact pads on degenerately doped $p+$ silicon substrates topped by 200 nm of thermal SiO_2 . An example of such a constriction is shown in Fig. 1(a). The metal, 1 nm of Ti (0.1 nm/s) and 15 nm of Au (0.2 nm/s), is deposited in an e-beam evaporator with base pressure of 10^{-7} mB. After liftoff the surface is cleaned by UV ozone for 5 minutes and O_2 plasma for 1 minute. Then 80 μ L of C_{60} in toluene solution (1 mg C_{60} / 1 mL toluene) are spin cast (spin speed ~ 900 RPM) onto the array of junctions. Scanning tunneling microscopy (STM) images of C_{60} deposited in this manner on an evaporated Ti/Au film show approximately monolayer coverage of the metal by the adsorbed molecules. An indium contact to the $p+$ silicon substrate, which serves as our back gate, is then made. The C_{60} -decorated junctions are placed in a variable temperature vacuum probe station (Desert Cryogenics) for the electromigration procedure and subsequent electrical characterization. The probe station is evacuated by turbomolecular pump (base pressure of probe station at 300 K is 5×10^{-5} mB) and cryopumped by a carbon felt sorption pump thermally anchored to the incoming cryogen line.

A two-step variation of the electromigration technique is employed to separate the constrictions into distinct source and drain electrodes. Using an HP

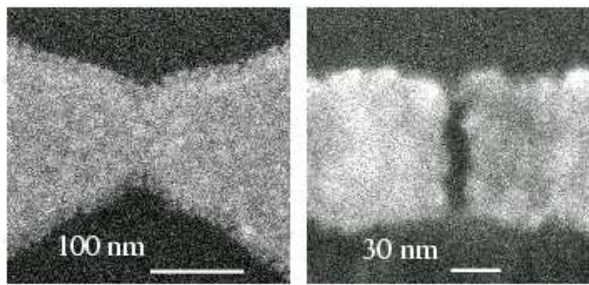


FIG. 1: (a) Scanning electron image of a 1 nm Ti/15 nm Au constriction defined by electron beam lithography on 200 nm SiO_2 on a degenerately doped $p+$ Si substrate (gate electrode). (b) A similar constriction after the electromigration procedure described in the text. The resulting interelectrode gap is less than 2 nm in this case.

4145B semiconductor parameter analyzer, at 300 K the voltage across each junction is ramped from 0 to 400 mV while monitoring the resulting current. When electromigration-induced junction breaking begins, indicated by decreased junction conductance, the maximum voltage across the junction is reduced in steps of 40 mV until the junction resistance is increased to 400-1000 Ω . Once each junction is “partially broken,” the sample is cooled to liquid helium temperatures. At 4.2 K the electromigration process is continued, with the maximum voltage ramps across the junction increased in steps of 200 mV as the junction conductance decreases. This process is halted when the resistance of the resulting electrodes is > 100 k Ω . This two-step electromigration technique allows us to make relatively high conductance electrodes consistently, which we infer corresponds to a very small interelectrode gap. Accurate scanning electron microscopy (SEM) assessment of the interelectrode gap is difficult because the newly exposed metal surfaces reconstruct when the electrodes are warmed back to room temperature. From SEM images of these resulting electrodes (Fig. 1(b)), we can see that the separation is less than 2 nm, the resolution of the SEM. Since the diameter of a C_{60} molecule is only 0.7 nm, closely spaced electrodes are essential for C_{60} SMTs.

Due to the stochastic nature of the electromigration process, every electrode pair differs at the atomic scale. Even if the closest interelectrode separation is the right size, the presence of a C_{60} molecule at that location is probabilistic, and depends strongly on the initial surface coverage of C_{60} . If a molecule is present, its couplings to the source, drain, and gate electrodes are determined by the microscopic arrangement of the junction region, which is different in every device. We know of no atomic-scale imaging technique at present that is capable of directly assessing in-situ the presence of an individual molecule between source and drain electrodes and the morphology of the gold electrodes adjacent to the molecule. Furthermore, the local charge environment of the SMT is unknown *a priori* due to the existence of surface trap states at the oxide surface. However, by analyzing many samples statistically we can estimate the per-

centage of the starting junctions that will become SMT given our fabrication procedure.

From a sample size of 1094 electrode pairs created using the above electromigration procedure, including control samples (no molecules; different solvent exposures; different cleaning procedures), 70% show measurable source-drain currents after electromigration at 4.2 K. We have examined 475 junctions decorated with C_{60} and electromigrated as described above. There are four classes of conductance characteristics in the resulting electrode pairs. (1) No detectable source-drain current at $|V_{\text{SD}}| = 0.1$ V (34%). The simplest explanation of these devices is that the breaking procedure resulted in significantly too large a source-drain separation to permit conduction. (2) Linear or slightly superlinear $I_{\text{D}} - V_{\text{SD}}$ curves, consistent with simple tunneling behavior with thermionic or field emission contributions at high bias (40%). The most likely explanation for these devices is that no molecule is present near the region of the source-drain gap that dominates conduction. (3) Nontrivial $I_{\text{D}} - V_{\text{SD}}$ curves with steps and abrupt changes in slope, but no detectable dependence on gate voltage, V_{G} (15.3%). These devices likely have a molecule or metal nanoparticle at the critical region of the interelectrode gap, but local geometry screens the object from the effects of the gate potential. (4) Nontrivial $I_{\text{D}} - V_{\text{SD}}$ curves that may be tuned significantly by varying V_{G} (10.7%). Conduction in these devices may be examined as a function of V_{G} , V_{SD} , and T , and compared with expectations for Coulomb blockade dominated single-molecule transistors. Occasionally some electrode pairs that initially have linear or nongateable $I_{\text{D}} - V_{\text{SD}}$ characteristics can change to exhibit interesting conductance features upon thermal cycling to 300 K and back to 4.2 K. Presumably this is results from a combination of molecular rearrangement and metal reconstruction at 300 K.

In a single-molecule transistor in the Coulomb blockade regime, the energetic cost of adding (removing) an electron to (from) the molecule, given by the Coulomb charging energy of the molecule and the energy difference between molecular levels, is sufficiently large, and the coupling between molecules and leads is sufficiently poor, that at most gate voltages the average charge on the molecule is fixed. The result of this charge quantization is a conductance gap, a region of V_{SD} near zero bias where the conductance is suppressed. The energetic alignment of the molecular orbitals with respect to the Fermi levels of the source and drain electrodes is determined by: the work function of the metal; the electron affinity of the molecule; the presence of any nearby charged defects or traps; and the capacitive coupling to the gate electrode. Because of this gate coupling, the size of the conductance gap varies linearly and reversibly with V_{G} , since a more positive value of gate voltage makes it energetically favorable to add an electron to the molecule. At biases larger than the conductance gap, conduction is permitted because the source-drain potential difference is sufficient to overcome the electron addition (subtrac-

tion) energy. At certain values of gate voltage (charge degeneracy points), it becomes energetically degenerate for the charge of the molecule to change by one electron. The result is that the conductance gap vanishes at zero bias, and as V_G is increased through such a charge degeneracy point, the average number of electrons on the molecule is increased by one. Because of the extremely small size of the molecule, the Coulomb charging energy of the molecule and the single-particle level spacing are both large ($\gg 100$ meV).

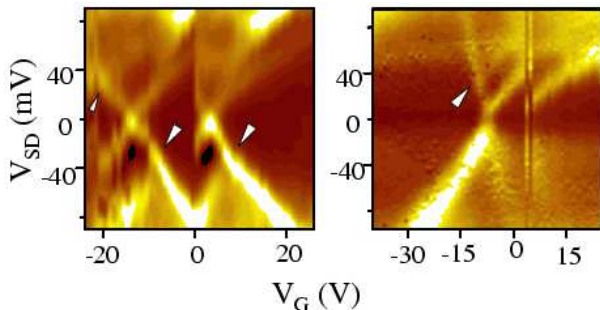


FIG. 2: Color maps of the differential conductance $\partial I_D/\partial V_{SD}$ as a function of gate and source-drain voltage, for two C_{60} single-molecule transistors (black = 0 S; white (left) = 4×10^{-6} S; white (right) = 1.2×10^{-5} S, $T = 4.2$ K). The “resetting” of the V_G axis is due to uncontrolled changes in the molecular charge environment due to nearby traps in the oxide. Moving from left to right along the V_G axis across the charge degeneracy point changes the average charge on the molecule by one electron. The arrows indicate the 35 meV vibrational resonance previously reported in Ref. [1].

Previous investigations of single-molecule transistors[1, 2, 3, 4] and other molecular devices[17] have reported additional resonances in the differential conductance at finite bias, corresponding to excitations of molecular vibrational modes during the transport process. For C_{60} devices[1], excitations of both the molecule-surface binding oscillation (~ 5 meV) and a mode intrinsic to the C_{60} have been reported (~ 35 meV). To characterize the electronic conduction in a SMT at a fixed temperature, it is useful to plot the differential conductance, $\partial I_D/\partial V_{SD}$, as a function of V_{SD} and V_G . The data shown here were acquired by measuring I_D as a function of V_{SD} for each value of V_G using the HP 4145B semiconductor parameter analyzer. The differential conductance is obtained by numerically differentiation of this data, using Savitzky-Golay smoothing to help reduce the noise in the resulting curves at the cost of V_{SD} resolution. For a given temperature the resulting differential conductance is plotted as a function of V_{SD} and V_G in a conductance contour map, where the color of the map represents different levels of conductance.

It is clear that not all gateable devices are C_{60} SMTs because about 5% of control samples (with no molecules) show some gateability. Approximately half the gateable control samples have clear Coulomb blockade style transport features, and the significant majority of these are consistent (charging energy ~ 30 meV; many acces-

sible charge states) with metal islands left behind following electromigration. The existence of these metal islands has been confirmed by SEM imaging. However, in two control devices on one substrate we observed Coulomb blockade features with charging energies as large as 400 meV, though no apparent vibrational excited levels. It is conceivable that some unintended adsorbed molecules contaminated this particular set of devices during the preparation process.

We have developed criteria for deciding if a particular device with nontrivial and gateable conductance is a SMT. The existence of Coulomb blockade is necessary but not sufficient. The charging energy of the Coulomb blockade feature must be relatively large, > 100 meV (This is a challenging experimental requirement, because device stability can be poor at such large biases.). The number of accessible charge states should be reasonable, in light of solution-based electrochemical redox information about the molecule. Finally, the existence of one or more vibrational resonances characteristic of the molecule (*e.g.* 35 meV for C_{60}) in the conductance map is the most indicative evidence that the device is a SMT. The conductance maps of two devices meeting these criteria are shown in Fig. 2. Note that the existence of surface trap states with charges that vary in time leads to instability in some devices. The random changes of the local charge environment near the tips of the electrodes contribute to some of the difficulties we have in observing the 35 meV vibrational state. In some of devices there appear to be multiple Coulomb blockade features overlapping each other, possibly due to the presence of multiple molecules between the electrodes.

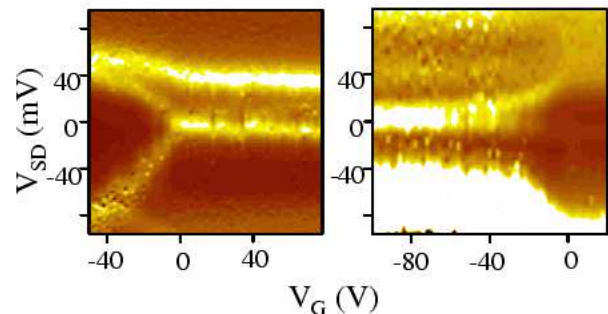


FIG. 3: Conductance maps for two devices showing apparent Kondo behavior, manifested as the appearance of a zero bias conductance peak in one molecular charge state. Note the presence of ~ 35 meV sidebands persisting into the Kondo regime. (dark = 0 S; white (left) = 1.5×10^{-5} S; white (right) = 6×10^{-7} S; $T = 4.2$ K)

Four of the devices successfully electromigrated at 4.2 K exhibit data like that shown in Fig. 3. When a transition is made from one charge state to another, a zero bias resonance appears in the differential conductance. Although a zero bias resonance is occasionally seen in control samples, the feature is always gate independent. The transitional behavior from Coulomb blockade to zero bias resonance is *never* observed in devices made without C_{60} molecules. This transition is consistent with the

Kondo effect in single-electron devices, where the Kondo resonance can only exist when the active region of the device has an odd number of electrons.

When describing Kondo phenomena in single-electron devices, the width of the localized state, Γ , is defined as the sum of the level widths due to the couplings, Γ_S, Γ_D of the localized state to the source and drain, respectively. The energy difference between the localized state (tunable by gate voltage) and the Fermi level of the leads is $-\epsilon$. When $0 < \epsilon/\Gamma < 1$, the system is said to be in the ‘‘mixed-valence’’ regime, while $\epsilon/\Gamma \gg 1$ corresponds to the Kondo regime. In this limit, the Kondo temperature is given[18, 19] by $T_K = 0.5(\Gamma U)^{1/2} \exp(-\pi\epsilon/\Gamma)$.

Note that T_K depends *exponentially* on Γ , and in a single-molecule transistor Γ depends *exponentially* on the relative position of the molecule with respect to the leads. This steep dependence has made it extremely challenging to examine this physics over a large temperature range, due to temporal instability of the molecule-metal configuration. For example, in one device of the type shown in Fig. 3, while acquiring conductance data the device switched irreversibly from exhibiting a Kondo-like zero bias peak, as shown, to standard Coulomb blockade of the type shown in Fig. 2, without a change in the charge degeneracy point. Within the Kondo picture, this change corresponds to the molecule-lead coupling changing to lower T_K below T . We have been able to acquire data over a limited temperature range for two devices exhibiting the Kondo-like resonance.

To analyze the zero bias resonance data in the context of Kondo physics, we follow previous SMT Kondo investigations[3, 4]. The Kondo temperature may be inferred in two different ways. First, assuming spin-1/2, at fixed gate voltage the zero bias conductance G may be monitored as a function of temperature, and fit with the formula $G(T) = G_0/(1 + 2^{1/s}T^2/T_K^2)^s$, where G_0 is a constant and $s \sim 0.22$ in the Kondo regime[19]. In both devices mentioned above, $G(T)$ is nearly constant, decreasing only slightly from 4.2 K up to ~ 30 K. This is consistent with large Kondo temperatures, $T_K > 100$ K, though the data do not put an upper bound on T_K .

Further analysis is possible making use of the conductance maps. Consider the device shown in Fig. 4. The slopes of the Coulomb blockade gap edges approximately give α , the conversion factor between gate voltage and the source-drain bias energy scale. For this sample, $\alpha \approx 2$ meV/ V_G , not surprising given the 200 nm thickness of the gate oxide. As $T \rightarrow 0$, the width of the zero bias Coulomb blockade conductance peak as a function of gate voltage saturates to $\Gamma \approx 32$ meV. Using α , and knowing that $\epsilon = 0$ at the charge degeneracy point, we can find $\epsilon(V_G)$. In a Kondo device the full-width at half maximum of the zero bias conductance peak is expected to be[3, 4, 12, 13, 14, 20] $\sim k_B T_K/e$. Fig. 4 shows this FWHM as a function of ϵ/Γ for that particular device. As with $G(T)$, this data is, within the noise, nearly temperature independent below 20 K, and an average of several low temperatures is plotted. This FWHM increase as

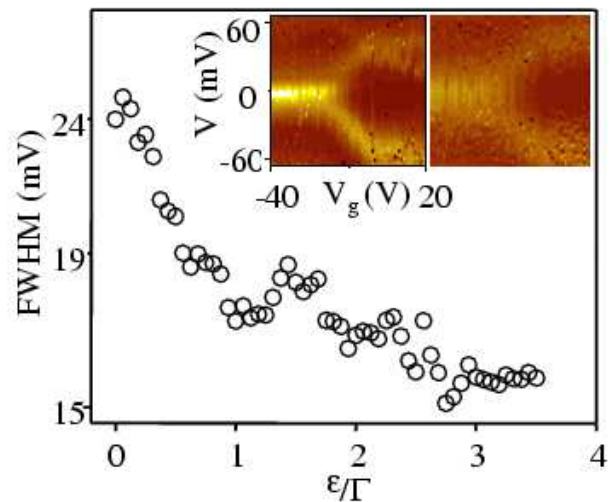


FIG. 4: A plot of full-width at half maximum of the zero bias conductance peak as a function of $\epsilon/\Gamma \propto |V_G - V_c|$, where V_c is the gate voltage of the charge degeneracy point. Inset: the conductance map of this device at 18 K (left) and 50 K (right), showing the persistence of the zero bias peak to quite high temperatures (dark = 0 S; white = 1.15×10^{-5} S).

$\epsilon \rightarrow 0$ is consistent with the Kondo behavior reported by Liang *et al.*[4]. The high effective Kondo temperatures implied by this data are clear from the insets to Fig. 4, which demonstrate that the zero bias resonance is still visible up to at least 50 K.

Other studies of the Kondo effect in single-molecule devices[3, 4] were able to demonstrate the Zeeman splitting of the Kondo resonance in an applied magnetic field. Because of the large intrinsic width (~ 10 -20 meV) of the zero bias resonance (consistent with high Kondo temperatures) that we observe, and the small size of the Zeeman splitting (115 μ eV per Tesla for a free electron), this would be extremely difficult to observe in our samples.

We also note that sidebands appear in these samples parallel to the zero bias peak. In the two samples shown in Fig. 3, the sidebands are located at $V_{SD} \sim 35$ meV, and appear to evolve from the inelastic resonances ascribed to vibrational excitations during the tunneling process. Hints of this behavior were noted in Ref. [4], but here there is coincidence of the sideband voltage and the known molecular vibrational resonance. Conductance under these nonequilibrium conditions would involve some interplay between inelastic processes and the coherent many-body Kondo state.

We have successfully created C_{60} -based single-molecule transistors using the electromigration technique[16]. Statistics on success are comparable to those reported by other investigators, and have been presented in detail, along with a discussion of controls and protocols. We find evidence of Kondo physics with large Kondo temperatures in some of these SMTs without having a metal ion present in the molecule. As mentioned above, sideband resonances indicate conduction processes that involve both many-body correlations and inelastic coupling to vibrational modes. Finally, we note that a high

temperature Kondo resonance in C_{60} adsorbed on a noble metal electrodes would explain the surprisingly narrow local density of states observed in scanning tunneling microscopy experiments with C_{60} tips[21].

The authors gratefully acknowledge the support of the Robert A. Welch Foundation, the Research Corporation,

and the David and Lucille Packard Foundation. The authors also thank K. Kelly and A. Osgood for STM characterization, and P.L. McEuen, P. Nordlander, H. Park, D.C. Ralph, A. Rumberg, J.M. Tour, and R.L. Willett for useful conversations.

-
- [1] Park, H.; Park, J.; Lim, A.; Anderson, E.; Alivisatos, A.; McEuen, P. *Nature* **2000**, *407*, 57–60.
- [2] Park, J.; Pasupathy, A.; Goldsmith, J.; Soldatov, A.; Chang, C.; Yaish, Y.; Sethna, J.; Abruna, H.; Ralph, D.; McEuen, P. *Thin Solid Films* **2003**, *438*, 457–461.
- [3] Park, J.; Pasupathy, A. N.; Goldsmith, J. I.; Chang, C.; Yaish, Y.; Petta, J. R.; Rinkowski, M.; Sethna, J. P.; Abruna, H. D.; McEuen, P. L.; Ralph, D. C. *Nature* **2002**, *417*, 722–725.
- [4] Liang, W.; Shores, M. P.; Bockrath, M.; Long, J. R.; Park, H. *Nature* **2002**, *417*, 725–729.
- [5] Grabert, H., Devoret, M. H., Eds. *Single Charge Tunneling: Coulomb Blockade Phenomena in Nanostructures*, NATO ASI series B: Physics Vol. 294; Plenum: New York, 1992.
- [6] Sohn, L. L., Kouwenhoven, L. P., Schön, G., Eds. *Mesoscopic Electron Transport*; Kluwer Academic Publishers: Dordrecht, the Netherlands, 1997.
- [7] Kondo, J. *Prog. Theor. Phys.* **1964**, *32*, 37–49.
- [8] Ng, T.; Lee, P. *Phys. Rev. Lett.* **1988**, *61*, 1768–1771.
- [9] Glazman, L.; Raikh, M. *JETP Lett.* **1988**, *47*, 452–455.
- [10] Meir, Y.; Wingreen, N.; Lee, P. *Phys. Rev. Lett.* **1993**, *70*, 2601–2604.
- [11] Wingreen, N.; Meir, Y. *Phys. Rev. B* **1994**, *49*, 11040–11052.
- [12] Goldhaber-Gordon, D.; Shtrikman, H.; Mahalu, D.; Abusch-Magder, D.; Meirav, U.; Kastner, M. *Nature* **1998**, *391*, 156–159.
- [13] Cronenwett, S.; Oosterkamp, T.; Kouwenhoven, L. *Nature* **1998**, *281*, 540–544.
- [14] Nygård, J.; Cobden, D.; Lindelof, P. *Nature* **2000**, *408*, 5824–5827.
- [15] Liang, W.; Bockrath, M.; Park, H. *Phys. Rev. Lett.* **2002**, *88*, 126801–1–126801–4.
- [16] Park, H.; Lim, A. K. L.; Alivisatos, A. P.; Park, J.; McEuen, P. L. *Appl. Phys. Lett.* **1999**, *75*, 301–303.
- [17] Zhitenev, N. B.; Meng, H.; Bao, Z. *Phys. Rev. Lett.* **2002**, *88*, 226801–1–226801–4.
- [18] Haldane, F. *Phys. Rev. Lett.* **1978**, *40*, 416–419.
- [19] Goldhaber-Gordon, D.; Gores, J.; Kastner, M.; Shtrikman, H.; Mahalu, D.; Meirav, U. *Phys. Rev. Lett.* **1998**, *81*, 5225–5228.
- [20] van der Wiel, W.; Franceschi, S. D.; Fujisawa, T.; Elzerman, J.; Tarucha, S.; Kouwenhoven, L. *Science* **2000**, *289*, 2105–2108.
- [21] Kelly, K.; Sarkar, D.; Hale, G.; Oldenburg, S.; Halas, N. *Science* **1996**, *273*, 1371–1373.